Earthquakes and Structures, *Vol. 9, No. 6 (2015) 1233-1250*
DOI: http://dx.doi.org/10.12989/eas.2015.9.6.1233

Experimental behavior and shear bearing capacity calculation of RC columns with a vertical splitting failure

Peng Wang*, Qing X. Shi, Qiu W. Wang and Yi Tao

School of Civil Engineering, Xi'an University of Architecture and Technology, Xi'an, China

(Received March 24, 2015, Revised July 16, 2015, Accepted October 10, 2015)

Abstract. The behavior of reinforced concrete (RC) columns made from high strength materials was investigated experimentally. Six high-strength concrete specimen columns (1:4 scale), which included three with high-strength transverse reinforcing bars and three with normal-strength transverse reinforcement, were tested under double curvature bending load. The effects of yielding strength and ratio of transverse reinforcement on the cracking patterns, hysteretic response, shear strength, ductility, strength reduction, energy dissipation and strain of reinforcement were studied. The test results indicated that all specimens failed in splitting failure, and specimens with high-strength transverse reinforcement exhibited better seismic performance than those with normal-strength transverse reinforcement. It also demonstrated that the strength of high-strength lateral reinforcing bars was fully utilized at the ultimate displacements. Shear strength formula of short concrete columns, which experienced a splitting failure, was proposed based on the Chinese concrete code. To enhance the applicability of the model, it was corroborated with 47 short concrete columns selected from the literature available. The results indicated that, the proposed method can give better predictions of shear strength for short columns that experienced a splitting failure than other shear strength models of ACI 318 and Chinese concrete codes.

Keywords: high-strength concrete columns; high-strength transverse reinforcement; splitting failure; quasi-static test; seismic behavior; strain of reinforcement; shear strength

1. Introduction

There can be many cases causing the appearance of short column effect within a structure, such as oversized cross sectional dimensions of columns, structure with staggered stories, setting infill walls between two columns and so on. Short columns at the ground storey of the structures are prone to brittle shear failure which may result in severe damages or even collapse because of the poor ductility during earthquakes (Guevara and García 2005a, Caglar and Mutlu 2009, Cagatay *et al*. 2010a, Chen *et al*. 2010b, Koçak 2013a). Many earthquake reconnaissance studies and experimental results have revealed that splitting failure is one of typical failure patterns for short RC columns. Generally, failure modes of RC columns mainly include flexural failure, shear failure and splitting failure. Considerable studies have been devoted to understanding the seismic behavior of RC columns with a flexural failure or a diagonal shear failure, while there are few

*Corresponding author, Ph.D., E-mail: jdwp0822@sina.cn

 ISSN: 2092-7614 (Print), 2092-7622 (Online)

studies on the seismic response of RC columns that experienced a splitting failure.

Splitting failure has attracted the attention of researchers since the 1970s, when researchers in Japan found that nearly 1/3 of 260 specimens failed to split along intermediate longitudinal reinforcing bars. Pham and Li (2013b, 2014a, 2014b), conducted the experiment studies on RC columns under simulated seismic load and constant axial load, and the test results indicated that a majority of the specimens experienced splitting failure. Sato and Kaminosono (1992) tested high-strength concrete columns with high-strength stirrups focusing on the behavior mechanism of the specimens, and the results indicated that remarkable vertical splitting occurred in the seismic test of specimens. The lateral load carrying capacity decreased significantly due to the formation of vertical splitting cracks. Splitting failure was also observed in tests of RC columns conducted by Tran and Li (2012a), Aoyama (2001a), Gupta and Collins (2001b), Sun *et al*. (2011). Studies by Ichinose (1995) and Lura *et al*. (2002) demonstrated that splitting failure is related to bonding failure, which occurred when the local bond strength of longitudinal reinforcing bars exceeded the bond stress capacity. Pandey and Mutsuyoshi (2005b) tested 15 RC columns to examine the influence of bond between longitudinal reinforcement and concrete on seismic behavior of the test specimens, and the test results demonstrated that the failure mode of the test specimens at the ultimate state could be changed from shear to flexure by reducing the bond strength of the longitudinal reinforcing bars. Mohamed and Farid (2008a) tested 12 RC columns using fibre-reinforced polymer (FRP) wraps to examine the effectiveness of strengthening method on behavior of bond-critical regions. It was found that confining the spliced zone with FRP wraps increased the bond strength of the spliced bars, reduced the bond deterioration and pinching under cyclic loading, and increased the lateral load resistance and ductility of the columns. Bhayusukma and Tsai (2014c) and Paultre *et al*. (2001c) conducted experimental studies on seismic behavior of high-strength concrete columns laterally reinforced with high-strength steel bars, the test results demonstrated that high-strength lateral reinforcement was quite effective in improving the ductility of high strength concrete columns.

However, there is still limited understanding about the behavior mechanism of RC columns that experienced splitting failure. The effect of factors on the seismic behavior of short RC columns is still far from being well understood. Moreover, columns that experienced splitting failure have poor deformation and energy dissipation capacity. And there is a sudden loss of shearing capacity right after the maximum lateral load was attained, especially in the case of columns with low ratio of transverse reinforcement or under a high axial compression ratio. Therefore, there is a need to investigate the behavior mechanism of columns that experienced splitting failure clearly.

This paper contributes to further understanding of seismic behavior of RC columns that experienced a splitting failure. An experimental program was carried out on six high-strength concrete columns under double curvature bending load and constant axial load. The specimen parameters were yielding strength and ratio of transverse reinforcement. The performance of specimens was discussed in terms of crack pattern, hysteretic response, ductility, strength reduction, energy dissipation and strain of reinforcement. Finally, the shear strength formula of short columns that experienced a splitting failure was proposed based on the Chinese code.

2. Experimental program

2.1 Description of test specimens

Six 1/4-scale concrete columns with deformed longitudinal reinforcing bars, which included three columns with high-strength transverse reinforcement and three with normal-strength lateral bars, were fabricated and tested under a combination of constant axial load and reversed cyclic load, and details of the specimens are shown in Fig. 1 and Table 1. Yielding strength and ratio of transverse reinforcement were chosen as test parameters in this study. All columns were designed to have a same cross section of 250 mm×250 mm. And the clear height of specimens was set to be 750 mm, resulting in a aspect ratio of λ=1.5. The test specimens were cast vertically using fine aggregate commercial concrete, and the cubic concrete compressive strength measured at the 28th day was 59.27 MPa. The test specimens were reinforced with twelve C12 reinforcing bars, and the ratio of longitudinal reinforcement was 2.17%. Grade HRB400 steel bars were used as the longitudinal steel bars with a design yielding strength of 360 MPa. The transverse reinforcement, which comprised of normal-strength steel bars and high-strength steel bars with 135-degree hooks extending with the length of 8 times the hoop diameters, were used in the test specimens, and they had yielding strengths of 464.7 MPa and 1143.3 MPa, respectively. The properties of steel bars are tabulated in Table 2. A well-shaped stirrup was used in all of the column specimens in order to prevent stirrup from decoupling during loading.

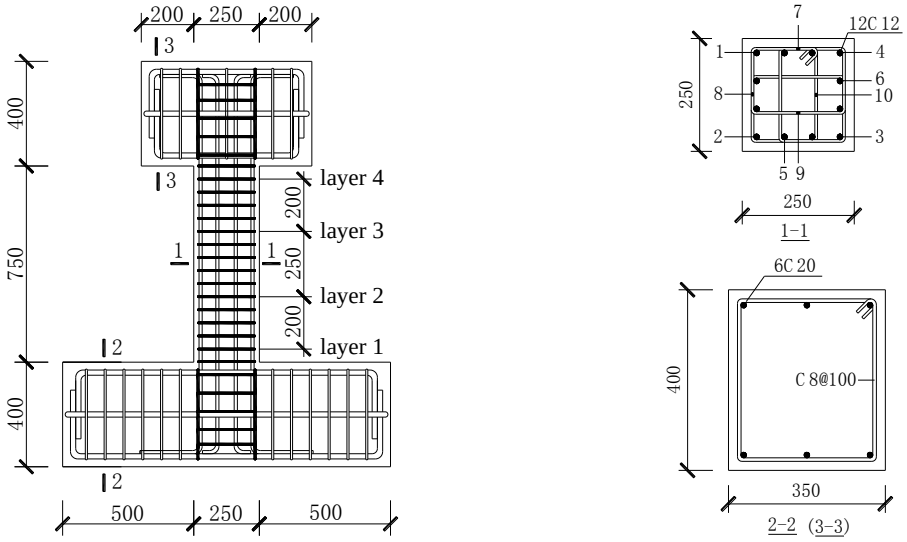

Fig. 1 Dimensions of the specimen

Table 1 Summary of test specimens

Specimen	b /mm	h /mm	L /mm	λ	A_s /mm^2	N/f_cA	Stirrups configuration			
							f_{yv} /MPa	D /mm	s /mm	ρ_s /%
DNC-1	250	250	750	1.5	1356	0.5	464.7	8	80	1.0
DHC-1	250	250	750	1.5	1356	0.5	1143.3	7	60	1.0
DNC-2	250	250	750	1.5	1356	0.5	464.7	8	60	1.34
DHC-2	250	250	750	1.5	1356	0.5	1143.3	7	46	1.34
DNC-3	250	250	750	1.5	1356	0.5	464.7	6	60	0.75
DHC-3	250	250	750	1.5	1356	0.5	1143.3	5	42	0.75

Table 2 Properties of steel bars

Bar Grade	Diameter /mm	Yield strength f_y /MPa	Ultimate strength f_u /MPa	Elongation δ_u /%	Elastic modulus E_s /10^5MPa	Bar type
HRB400	5.9	455.8	639.4	18.26	2.0	plain
	8.0	485.5	650.4	23.83	2.0	deformed
	12.0	464.7	628.4	26.41	2.0	deformed
High-strength	4.95	1182.6	1203.4	10.2	2.0	plain
	7.0	1143.3	1167.2	9.14	2.0	deformed

2.2 Testing procedure

Low cyclic reversed loading was applied to each specimen while axial compression was held constant. The test setup is shown in Fig. 2. Parallelogram linkage was used to maintain the boundary condition of zero rotation at the top of the specimen. A horizontal actuator was used to provide lateral force to the top end of the test columns, and the actuator was pinned at both ends to allow rotation during the test. The lateral load was applied cyclically through the horizontal actuator in a quasi-static fashion, as shown in Fig. 3. The base of the specimens was fixed to a strong floor held by four post-tensioned high strength bolts. A load-displacement hybrid control program was applied, in which the lateral loading sequence was controlled by force for the initial loading cycles till the yielding initiation of the test specimen was observed. This observation was accomplished by monitoring the reaction forces of the MTS horizontal actuator. From 50 kN, every load level was applied for 1 cycle in an increment of 50 kN. When loaded to the yielding force, the loading sequence was controlled by displacement. Then, the target displacements for the cyclic loading were set as the multiple of the yield displacement(Δ_y), the cyclic loadings were repeated three times at each displacement level. The test was terminated until the reaction force descended to about 50% of the maximum load.

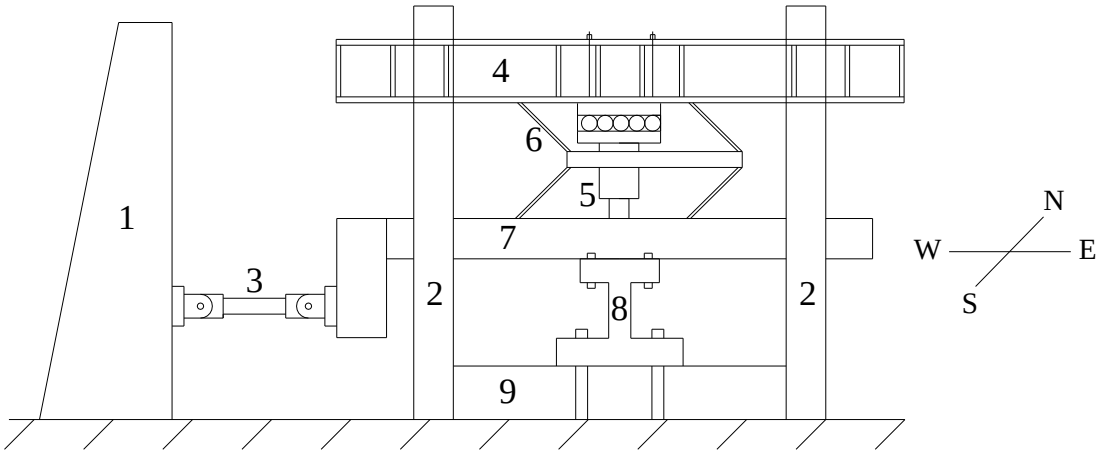

1. Reaction wall. 2. Reaction steel frame. 3. 500 kN horizontal actuator. 4. Reaction girder.
5. Vertical hydraulic jack. 6. Parallelogram linkage. 7. L-shaped beam. 8. Specimen. 9. Strong floor

Fig. 2 Test setup

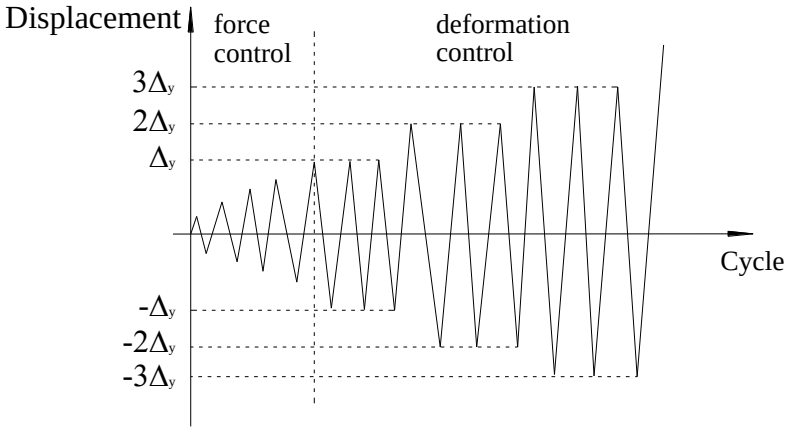

Fig. 3 Loading procedure

2.3 Instrumentations

The test specimens had been extensively installed with measuring devices both internally and externally. Lateral displacement was measured by two horizontal LVDTs parallel to the horizontal actuator, which were mounted at the top and bottom side of the bases, respectively. Shear and flexural deformation were obtained by readings of a number of LVDT sets mounted throughout the height of the specimens. Strain gages were mounted to capture the strain history in both longitudinal reinforcing bars and stirrups at critical positions, as shown in Fig. 1.

3. Specimen behavior

3.1 Cracking pattern

The final failure modes of specimens are shown in Fig. 4, which indicated that all specimens in this test experienced a vertical splitting failure. This vertical splitting spread through the interior of the specimen along inner transverse reinforcement, and separated it into three parts. It was confirmed that the vertical split penetrated the whole section and extended throughout, except at the both ends where the flexural hinge developed. The failure process was as follows.

Under an approximate 200 kN~280 kN, horizontal cracks were observed on the east and west sides, 150 mm above the base. These cracks spread slantingly in the south and north sides. Furthermore, vertical bond splitting cracks were formed along the mid-longitudinal bars, where was 250 mm away from the bottom end of the column, developing to both ends of the specimen. With the lateral drift increasing, cracks of the east and west sides at both ends developed into a horizontal penetrating crack. Moreover, some new cracks were observed and developed horizontally. The inclined cracks at both ends of the column developed towards the middle of the specimens with inclination angle increasing. Furthermore, some vertical cracks extended towards both ends of the columns. Under the cyclic lateral loading, a large number of micro-inclined cracks occurred and developed crossing each other along the length of the mid-bars.

Under cyclic loading of $1\Delta_y$ (Δ_y is the yield displacement), the corner cover concrete spalling

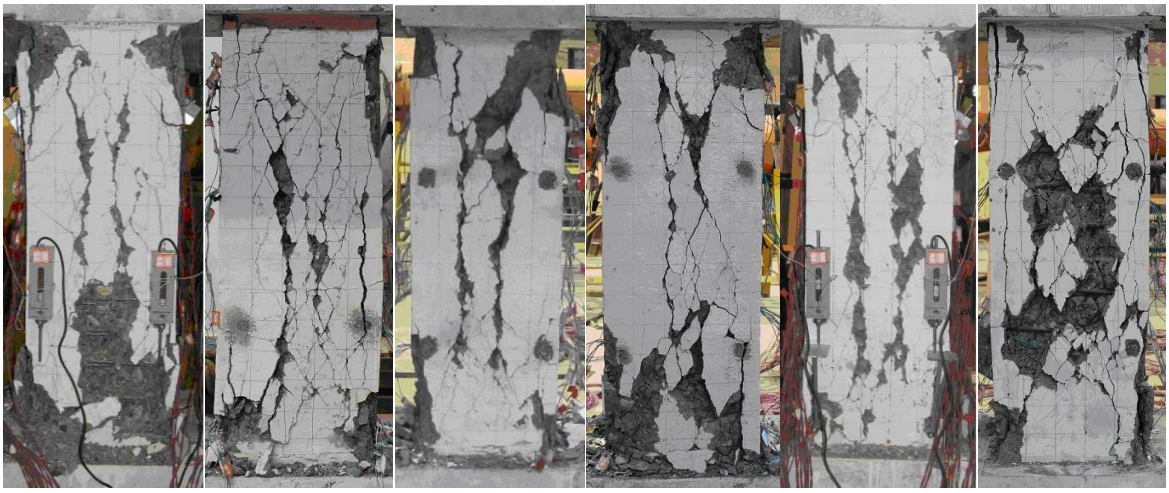

(a) DHC-1 (b)DNC-1 (c) DHC-2 (d)DNC-2 (e) DHC-3 (f) DNC-3

Fig. 4 Final failure modes of specimens

was developed at both ends of the columns. Oblique cracks of south and north sides extended further at both ends of the columns. Moreover, two vertical splitting cracks developed into main cracks due to the action of cyclic loading. Under cyclic loading of $2\Delta_y$, the width of main cracks increased. However, there was almost no new crack emerging. Under cyclic loading of $3\Delta_y$, main bond-splitting cracks in the south and north sides developed further toward both ends of the columns. And some cover concrete started to spall and be crushed at both ends of the columns. Under cyclic loading of $4\Delta_y$, cover concrete located at both flexural hinge zone was spalling severely. Some longitudinal steel bars were exposed after cover concrete spalling. But core concrete of specimens with high-strength stirrups was not crushed severely.

3.2 Hysteretic response

Generally, the hysteretic responses illustrate the pinching effect, stiffness degeneration, and strength reduction during repeated cyclic loading. Hysteretic responses obtained from the test are depicted in Fig. 5. Before reaching the yielding force, hysteretic curves of the specimens were narrow, with low energy dissipation, and the stiffness degradation was not obvious. After the yield force, with the increasing area of hysteretic loops, energy dissipation started to increase. When loaded to the same displacement, shear bearing strength of specimens in the last two cycles was lower than those in the first cycle. Fig. 5 also reveals that stirrup strength and stirrup ratio affected the hysteretic response significantly. With the same stirrup ratio, energy dissipation capacity and ductility of specimens confined with high-strength stirrups were superior to those with normal-strength lateral bars. After the maximum lateral force was attained, shearing capacity of specimen columns with normal-strength stirrups decreased faster than those of columns with high-strength stirrups, especially in the case of columns with a small transverse reinforcement ratio. Moreover, at a certain displacement level, shear bearing capacity of specimens with high-strength stirrups was more stable than those with normal-strength lateral bars in the last two cycles.

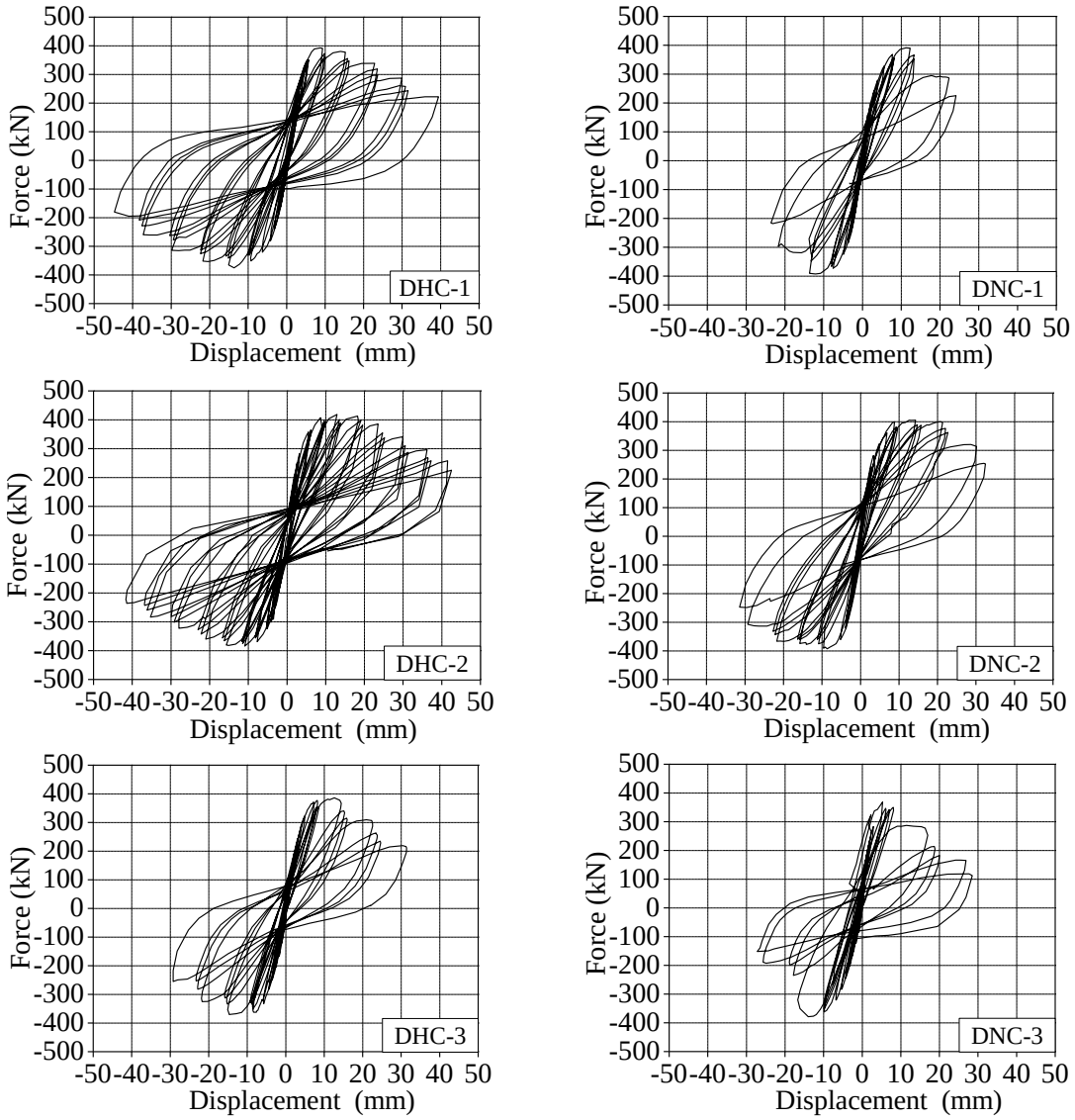

Fig. 5 Hysteretic response of test specimens

3.3 Backbone curves

Backbone curves obtained from the test are shown in Fig. 6, and it indicated that stirrup strength has little effect on the shear bearing capacity of short RC columns. However, the deformation capacity of specimens with high-strength stirrups was improved significantly, especially in the case of columns with a small transverse reinforcement ratio. By comparing among DNC-1, DNC-2 and DNC-3, it is noted that reducing stirrup spacing is a more efficient measure to improve the seismic behavior of concrete column than increasing the diameter of stirrups. Comparisons made between DHC-1 and DNC-2 demonstrate that two backbone curves

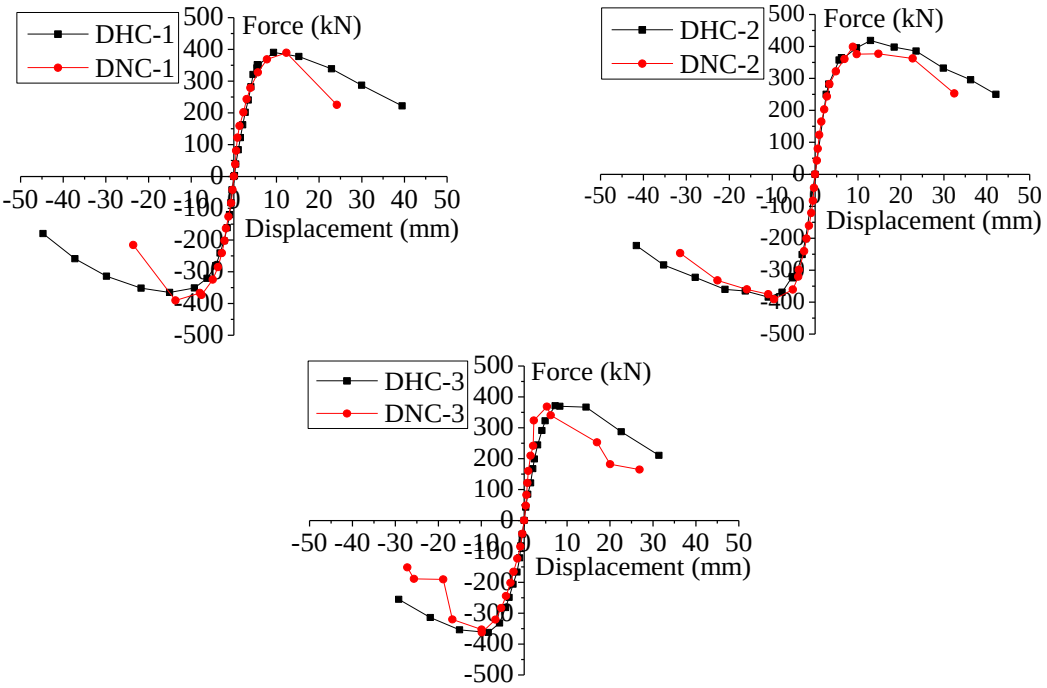

Fig. 6 Backbone curves of specimens

are quite similar in the peak lateral force and displacement ductility, above all, DHC-1 could save 30 percent of steel. Moreover, there was no steep reducing in shear bearing capacity of specimens with high-strength stirrups after the maximum lateral load was attained.

3.4 Ductility

Ductility illustrates deformation capacity of structure component after reaching the peak lateral force. In this paper ductility coefficient and ultimate drift were taken to describe the deformation capacity of the test specimens. Computational expressions were as follows

$$\mu_{\Delta} = \Delta_{\mathrm{u}} / \Delta_{\mathrm{y}} \tag{1}$$

$$\theta_{\mathrm{p}} = \Delta_{\mathrm{u}} / H \tag{2}$$

where μ_{Δ} is ductility coefficient, θ_{p} is ultimate drift ratio, Δ_{u} is ultimate displacement, Δ_{y} is yield displacement, and H is clear height of the specimen. The yield lateral force was defined by monitoring the MTS horizontal actuator and the yield displacement is the displacement at the yielding force. The ultimate displacement is the one where 80% of peak lateral load is sustained.

The cracking forces, yield forces, peak forces, ultimate forces and their corresponding displacements in both push and pull directions are shown in Table 3 (“positive value” and “negative value” represents the force or displacement in the push and pull directions, respectively.). It is noted that deformation capacity was improved significantly for specimens confined with high-strength stirrups. For example, the ultimate drift ratios are 1/57 and 1/37 for

Table 3 Test results of specimens under different loading stages

specimen	Crack		Yeild		Peak		Ultimate		μ_Δ		θ_p	
	Force /kN	Dis /mm	Force /kN	Dis /mm	Force /kN	Dis /mm	Force /kN	Dis /mm				
DHC-1	282	4.2	353	5.9	393	8.8	334	22.7	3.85	4.49	1/33	1/29
	-281	-4.2	-312	-5.8	-375	-13.7	-319	-29.7	5.12		1/25	
DNC-1	279	3.9	330	5.7	391	11.2	332	16.5	2.89	3.17	1/45	1/45
	-325	-4.9	-324	-4.9	-393	-12.1	-334	-16.9	3.45		1/44	
DHC-2	281	4.6	365	6.1	419	12.9	356	27.1	4.44	4.71	1/27	1/27
	-241	-3.3	-327	-5.6	-385	-10.9	-327	-27.9	4.98		1/26	
DNC-2	203	2.15	334	5.9	405	14.3	344	20.4	3.46	3.59	1/37	1/38
	-241	-2.15	-346	-5.3	-391	-9.6	-332	-19.7	3.72		1/38	
DHC-3	168	2.02	328	5.2	386	12.6	328	18.4	3.54	3.88	1/41	1/37
	-206	-2.6	-313	-5.2	-370	-14.7	-315	-21.9	4.21		1/34	
DNC-3	210	1.5	334	3.4	369	5.3	314	9.4	2.76	2.67	1/80	1/57
	-202	-3.2	-316	-6.5	-378	-14.0	-321	-16.7	2.57		1/45	

DNC-3 and DHC-3, respectively. And specimen DHC-3 exhibits good collapse resistant capacity. For specimens with high-strength stirrups, the ductility coefficient is increased by approximately 39.4%, while the ultimate drift ratio is increased by approximately 50.0%.

3.5 Strength reduction

Under the same displacement level, the strength of structure member decreased with the increasing loading cycles, and this phenomenon is called strength reduction. Generally, strength reduction can be expressed as V_n/V_1, where V_1 and V_n represent the maximum lateral load of the first and the n^{th} loading cycle in the same loading level, respectively. Fig. 7 shows the relationship between strength reduction and displacement, and it indicates that the yielding strength of transverse reinforcement affects strength degradation significantly, especially in the case of columns with a low transverse reinforcement ratio. After test specimens were observed yielding, a lot of concrete cracks occurred which leaded specimen strength starting to reduce. As the top displacement increasing, the speed of strength reduction is from slow to fast. However, the speed of strength degradation for columns which used high-strength transverse reinforcement is much more stable and slow than that of columns using normal-strength stirrups. Due to high yielding strength of high-strength transverse reinforcement, longitudinal reinforcing bars can be confined adequately. The mechanical behavior of concrete core is improved, so the strength reduction is alleviated. Fig. 7 also demonstrates that transverse reinforcement ratio is another important factor, which affects the behavior of strength reduction significantly. With the increasing of transverse reinforcement ratio, strength reduction becomes slow.

3.6 Energy dissipation capacity

Energy dissipation capacity is an important seismic performance index for structure or structure

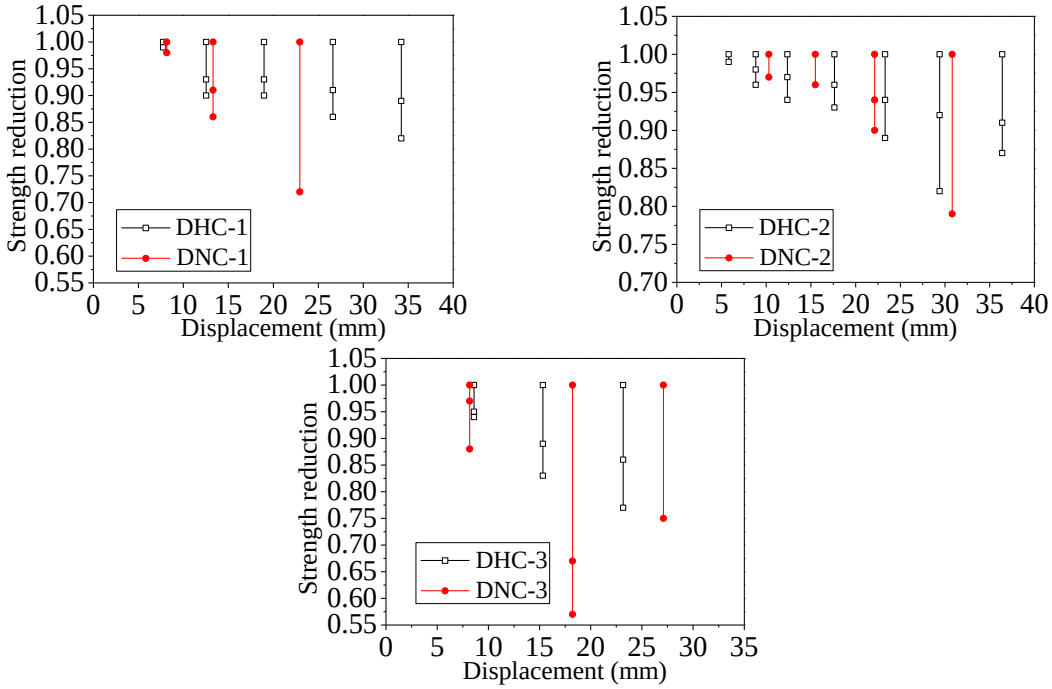

Fig. 7 Strength reduction

Table 4 Energy dissipation of specimen columns (kN·mm)

Dis. level	DHC-1		DNC-1		DHC-2		DNC-2		DHC-3		DNC-3	
	cycle times	Energy	cycle times	Energy	cycle times	Energy	cycle times	Energy	cycle times	Energy	cycle times	Energy
$1\Delta_y$	3	2310	3	2114	3	1372	3	3725	3	3270	3	3404
$2\Delta_y$	3	9088	3	10177	3	4302	3	11963	3	11034	3	13890
$3\Delta_y$	3	17461	2	15192	3	6362	3	21667	3	18977	2	14626
$4\Delta_y$	3	28067			3	12479	2	23152	1	9144		
$5\Delta_y$	3	39098			3	18101						
$6\Delta_y$	1	17450			3	26240						
$7\Delta_y$					3	31105						
$8\Delta_y$					1	14173						
Total energy		113474		27483		114134		60507		42425		31920

member, which is represented by cumulative energy dissipation in this paper. Table 4 shows the energy dissipation of test specimens obtained from test. Before the yielding lateral load was attained, energy dissipation was so small that it was neglected in the computation of energy dissipation. As the top displacement increasing, the area of hysteretic loop became larger gradually, and energy dissipation was increasing accordingly. From the table, it can be seen that cumulative energy dissipation is significantly increased with the increasing of transverse

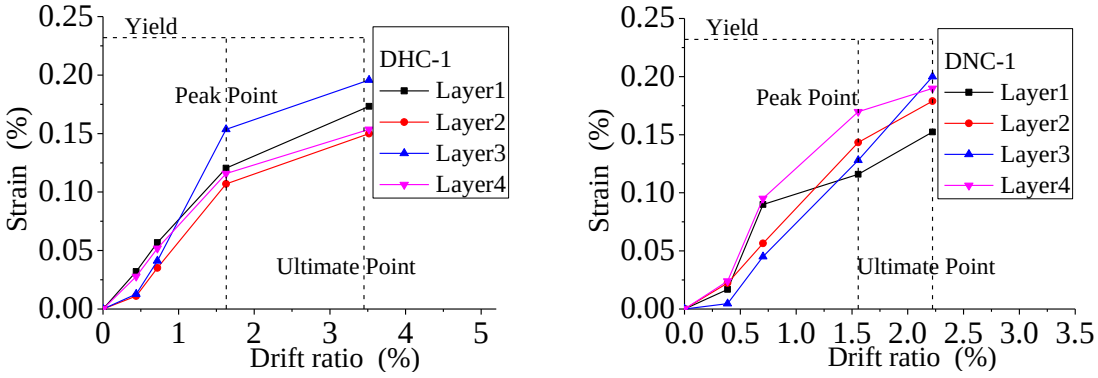

Fig. 8 Strain of longitudinal steel bars for specimens

(Note: strain value in Fig. 8 is the maximum strain value of the gauge readings in the same layer)

reinforcement ratio. At the same time, energy dissipation of specimens with high-strength stirrups is much larger than that of specimens which used normal-strength stirrups. With the transverse reinforcement ratio of 0.75%, 1.0% and 1.34%, energy dissipation of specimens with high-strength stirrups is increased by 32.9%, 310% and 90% respectively than that of specimens with normal-strength stirrups.

3.7 Strain of reinforcement

3.7.1 Strain of longitudinal reinforcing bars

Strain gauge readings indicate that no yielding of longitudinal reinforcing bars was observed for all specimens during the test. And surprisingly, it is noted that the strain patterns of all specimens were similar. Fig. 8 shows the variation of strains in longitudinal reinforcing bars at different drift ratios for specimen DHC-1 and DNC-1. For DHC-1 with high-strength stirrups, when loaded to a drift ratio of 1.6%, strains in longitudinal bars increased linearly. At a drift ratio of 1.6% (at the maximum shear strength), strain in longitudinal bars was in the range of 0.0011 and 0.00154, which was approximately 50% of the yield strain. After a drift ratio of 1.6%, strains in longitudinal bars increased relatively slow. For DNC-1 with normal-strength lateral bars, strains in longitudinal bars increased slowly until loading to a drift ratio of 0.386%. When loaded to a drift ratio of 1.55% (at peak shear strength), strain in longitudinal bars was in the range of 0.0012 and 0.0017, which was a little larger than those of DHC-1. DNC-1 reached ultimate damage state at a drift ratio of 0.0225, while DHC-1 experienced ultimate damage at a drift ratio of 0.0345 due to the effect of high-strength transverse reinforcement.

3.7.2 Strain of transverse reinforcing bars

Fig. 9 shows the variation of strains in lateral steel bars at different drift ratios for all specimens. At a drift ratio of approximate 0.8%, strains in all transverse reinforcements remained relatively low at an initial strain value. When loaded to a drift ratio of 0.8%, strains in lateral steel bars increased rapidly, especially in the case of specimens with normal-strength lateral bars. When loaded to the maximum shear force, transverse reinforcing bars had reached or been closed to yield strength for specimens with normal-strength lateral bars, while high-strength stirrups were far away from yielding. When loaded to ultimate shear force, there was no yielding of transverse steel

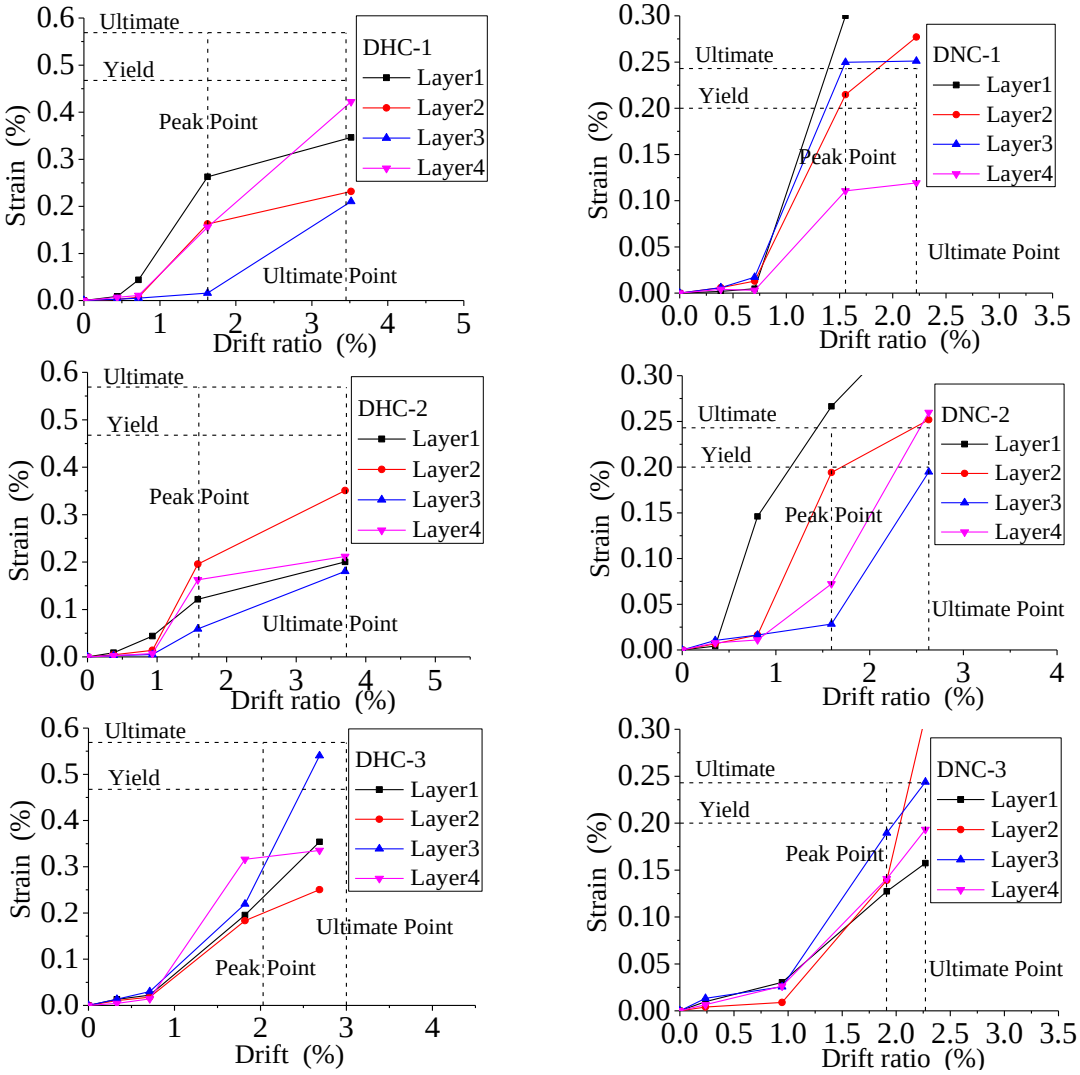

Fig. 9 Strain of stirrups for specimens

(Note: strain value in Fig. 9 is the maximum strain value of the gauge readings in the same layer)

bars observed for DHC-1 and DHC-2, while few stirrups reached yielding for DHC-3 due to a low ratio of transverse reinforcement. As expected of no yielding, core concrete could still be confined adequately by high-strength stirrups even after peak shear force. The results demonstrate that high-strength stirrups could afford adequate confinement of the longitudinal reinforcement even after the maximum shearing capacity was attained.

4. Shear bearing capacity

Although the behavior of RC members in shear has been studied for years, engineers are still

unable to determine the shear strength of RC columns accurately. The models and formulas of shear bearing capacity for RC columns are different among countries. The purely empirical shear strength model, which was adopted by Chinese current code (2010c), was based on the test specimens made from normal-strength materials, and its applicability for columns made from high-strength materials needed to be examined. On the other hand, for columns failed in diagonal shear, shear strength calculated based on the Chinese code method have a good agreement with test results, while the computation results are in poor agreement with the test results of columns that experienced a splitting failure, especially in the case of columns made from high-strength materials. Based on the Chinese code method, a computation formula, which can well predict the shear bearing capacity of columns experienced a splitting failure, was proposed by statistic analysis. The formula can be expressed as

$$V=\frac{1.05}{\lambda+1}f_{\mathrm{t}}bh_0+\rho_{\mathrm{s}}f_{\mathrm{yv}}bh_0+0.07N \tag{3}$$

where λ stands for shear span-depth ratio; f_{t} is the concrete tensile strength; b is the width of the computational cross-section; h_0 is the effective depth of the column cross section; ρ_{s} is the transverse reinforcement ratio; f_{yv} is the yielding strength of transverse reinforcing bars; N is the axial force. For columns with transverse reinforcement index $\rho_{\mathrm{s}}f_{\mathrm{yv}}$ larger than 4, $\rho_{\mathrm{s}}f_{\mathrm{yv}}$=4(1990a); and for columns with axial force N larger than $0.3f_{\mathrm{c}}A$, N=$0.3f_{\mathrm{c}}A$, where f_{c} is the concrete compressive strength; A represents the gross cross-sectional area of the column.

The verification of the proposed formula was demonstrated by comparison with experimental results with respect to the maximum shear strength obtained from the test results of 47 columns available. These specimens were selected mainly on the basis of the observed failure pattern, where splitting failure occurred. All of them were short columns with aspect ratio ranging from 1.5 to 2.5. These columns had sizes ($b\times h\times L$) ranging from 250×250×750 mm to 200×610×1700 mm. The concrete compressive strength ranged from 20.2 to 83.8 MPa, while the area ratio of transverse reinforcement ranged from to 0.13 to 1.34%. The yielding strength of transverse reinforcement ranged from 300 to 1143 MPa, and the applied axial load ratio ranged from 0.05 to 0.7. Details of these specimens and their calculated shear strength are tabulated in Table 5.

Shear strength estimations were also estimated based on the methods from current Chinese Code (2010c). And ACI 318 (2008b) and Chinese Code were compared to the proposed method. The shear bearing capacity, as defined in Chinese Code, is given as

$$V=\frac{1.75}{\lambda+1}f_{\mathrm{t}}bh_0+f_{\mathrm{yv}}\frac{A_{\mathrm{sv}}}{s}h_0+0.07N \tag{4}$$

where A_{sv} stands for the area of transverse reinforcement; and s is stirrup spacing. The shear strength, as defined in ACI 318, based on a 45-degree truss model, is given as

$$V_n=\frac{A_{\mathrm{v}}f_{\mathrm{yt}}d}{s}+\frac{1}{6}\left(1+\frac{P}{14A_g}\right)bd\sqrt{f_c'} \tag{5}$$

where A_{v} stands for the area of transverse reinforcement; f_{yt} is the yielding strength of transverse reinforcing bars; d is the effective depth of the column cross section; P is the axial force; A_{g} represents the gross cross-sectional area of the column; and f_{c}' is concrete compressive strength.

Table 5 Details of specimens and comparisons of shear strength calculated by different methods

Authors	Specimens	b (mm)	h (mm)	a/d	f_c' (MPa)	ρ_s (%)	f_{yv} (MPa)	n	V_{test} (kN)	V_{pro} (kN)	V_{Chi} (kN)	V_{ACI} (kN)
Current tests	DHC-1	250	250	1.5	50.2	1.00	1143	0.5	353	385.8	492.3	547.6
	DHC-2	250	250	1.5	52.5	1.34	1143	0.5	365	385.8	492.3	638.5
	DHC-3	250	250	1.5	48.5	0.75	1143	0.5	328	385.8	634.6	735.3
	DNC-1	250	250	1.5	52.4	1.00	456	0.5	330	387.5	795.5	851.8
	DNC-2	250	250	1.5	54.2	1.34	456	0.5	346	387.5	795.5	874.9
	DNC-3	250	250	1.5	51.0	0.75	456	0.5	334	387.5	795.5	874.9
Shi *et al.* (2012b)	HHSC2	250	250	1.5	64.3	0.63	998	0.5	361	438.8	657.8	585.2
	HHSC4	250	250	2	64.3	0.63	998	0.5	294	421.6	629.1	585.2
	HHSC5	250	250	1.5	71.4	1.05	998	0.5	419	438.8	934.8	871.3
	HHSC6	250	250	1.5	60.4	0.39	998	0.5	348	433.6	502.4	424.5
	HHSC8	250	250	1.5	74.8	0.63	998	0.5	439	462.8	688.7	634.2
	HHSC9	250	250	1.5	74.8	0.63	998	0.7	388	462.8	688.7	721.7
Sato, and Kaminosono (1992)	5	250	250	2	78.4	0.64	808.5	0.4	446.1	387.3	480.5	534.8
	6	250	250	2	78.4	0.64	808.5	0.6	466.1	338.6	770.6	835.7
	7	250	250	2	78.4	0.96	808.5	0.5	474.7	344.0	987.3	1054
	8	250	250	2	79.2	0.96	1109.2	0.4	466	334.6	611.2	783.5
	9	250	250	2	79.2	0.96	1109.2	0.45	475.2	249.1	335.3	172.1
	10	250	250	2	79.2	0.96	1109.2	0.45	475.2	270.5	355.0	172.1
	11	250	250	2.5	83.8	0.51	980.7	0.35	352.1	226.1	296.0	173.4
Pham and Li (2014a)	SP1-1.7-0.2	350	350	1.71	29.8	0.13	475	0.2	238.3	240.9	306.5	171.2
	SP2-1.7-0.35	350	350	1.71	29.2	0.13	475	0.35	263.2	268.8	337.5	200.7
	SP3-2.4-0.2	350	350	2.43	30.6	0.13	475	0.2	193.3	263.2	329.6	200.0
	SP4-2.4-0.35	350	350	2.43	28.7	0.13	475	0.35	198	281.1	354.8	224.8
	SR1-1.7-0.35	250	490	1.73	23.3	0.18	509	0.35	263	288.1	356.8	222.5
	SR2-1.7-0.5	250	490	1.73	22.5	0.18	509	0.5	272	290.4	360.1	224.1
	SW1-1.4-0.2	200	610	1.39	21.7	0.23	509	0.2	246.5	239.3	335.1	191.3
	SW2-1.4-0.35	200	610	1.39	20.2	0.23	509	0.35	266	269.1	348.1	184.4
	SW3-1.4-0.5	200	610	1.39	20.5	0.23	509	0.5	289	322.1	370.8	256.8
Tran and Li (2012a)	RC-1.7-0.05	250	490	1.73	32.5	0.18	392.6	0.05	283.1	194.1	238.5	167.0
	RC-1.7-0.5	250	490	1.73	26.8	0.18	392.6	0.5	355.2	274.1	332.6	233.0
Moretti and Tassios (2006)	Specimen7	250	250	2	38.0	1.21	300	0.3	210	303.5	396.3	316.1
Harumi *et al.* (1990b)	15-0.56@90-6B	250	250	1.5	28.8	0.57	378	0.08	158	205.4	250.4	167.6
	15-0.85@60-6B	250	250	1.5	38.0	0.85	378	0.06	198	218.2	263.2	168.0
	15-1.28@60-6B	250	250	1.5	31.4	1.27	378	0.08	185	343.9	487.0	319.6
	30-0.56@90-6B	250	250	1.5	29.2	0.57	378	0.16	250	348.0	574.5	406.0
	45-0.56@90-6B	250	250	1.5	29.2	0.57	378	0.26	240	308.6	422.4	255.9

Table 5 Continued

Authors	Specimens	b (mm)	h (mm)	a/d	f_c' (MPa)	ρ_s (%)	f_{yv} (MPa)	n	V_{test} (kN)	V_{pro} (kN)	V_{Chi} (kN)	V_{ACI} (kN)
Sun *et al.* (2011)	R5	300	300	2.5	40.9	0.47	511	0.23	234	322.0	417.5	324.9
	R6	300	300	1.5	40.7	0.24	511	0.05	218	195.3	347.4	211.4
	R7	300	300	1.5	41.7	0.31	511	0.05	230.5	234.2	383.2	249.9
	R8	300	300	1.5	38.9	0.31	511	0.14	295.7	246.5	383.8	247.1
	R9	300	300	1.5	40.9	0.47	511	0.23	374	342.7	476.5	324.9
	R11	300	300	2	41.9	0.31	511	0.14	235.6	241.9	366.9	250.8
	R12	300	300	2	40.9	0.47	511	0.14	268.9	312.6	424.1	324.3
	R13	300	300	2	34.3	0.24	511	0.14	193	187.9	291.8	203.8
	R14	300	300	2	42.6	0.24	511	0.14	230.8	207.0	340.4	214.2
	R16	300	300	2.5	33.0	0.31	511	0.14	163.9	214.4	294.9	239.3
	R17	300	300	2	33.0	0.31	511	0.14	237.7	221.4	315.3	239.3
								Ave(V_i/V_{test})		1.05	1.55	1.25
								COV(V_i/V_{test})		0.19	0.23	0.42

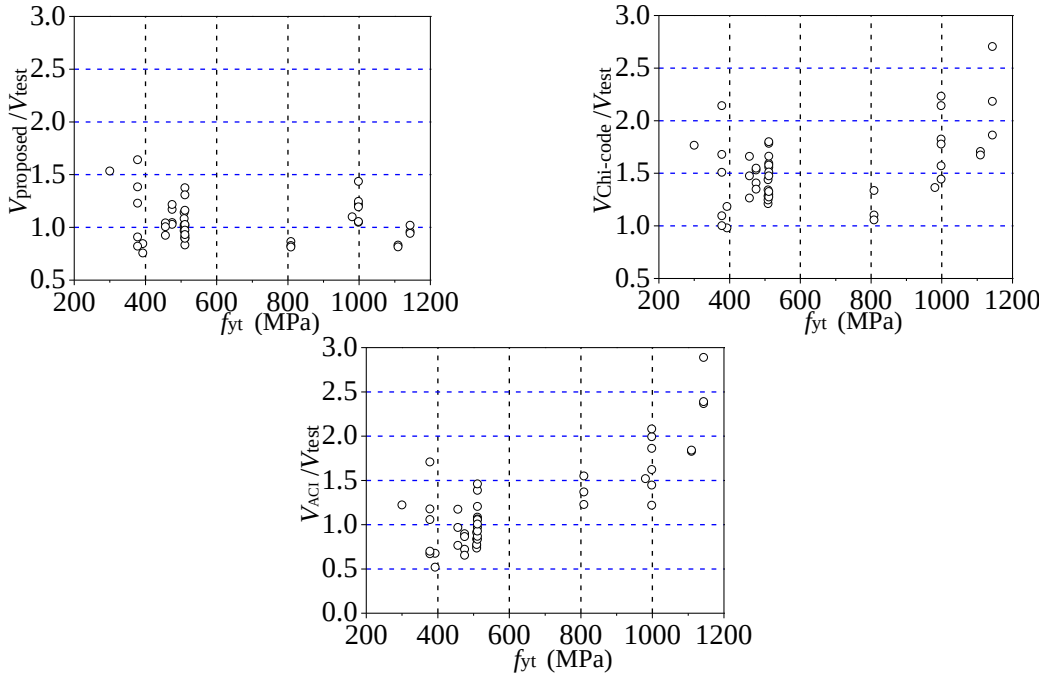

Fig. 10 Shear strength calculated based on different methods

Fig. 10 shows the comparisons of the tested shear strength with the calculated shear strength $V_{proposed}$, $V_{Chi\text{-}code}$ and V_{ACI}. The mean ratio of the measured to calculated shear strengths and its coefficient of variation are 1.05 and 0.19, 1.55 and 0.23, and 1.25 and 0.42 for the proposed method and methods from Chinese Code and ACI 318-08, respectively. It is noted that Chinese

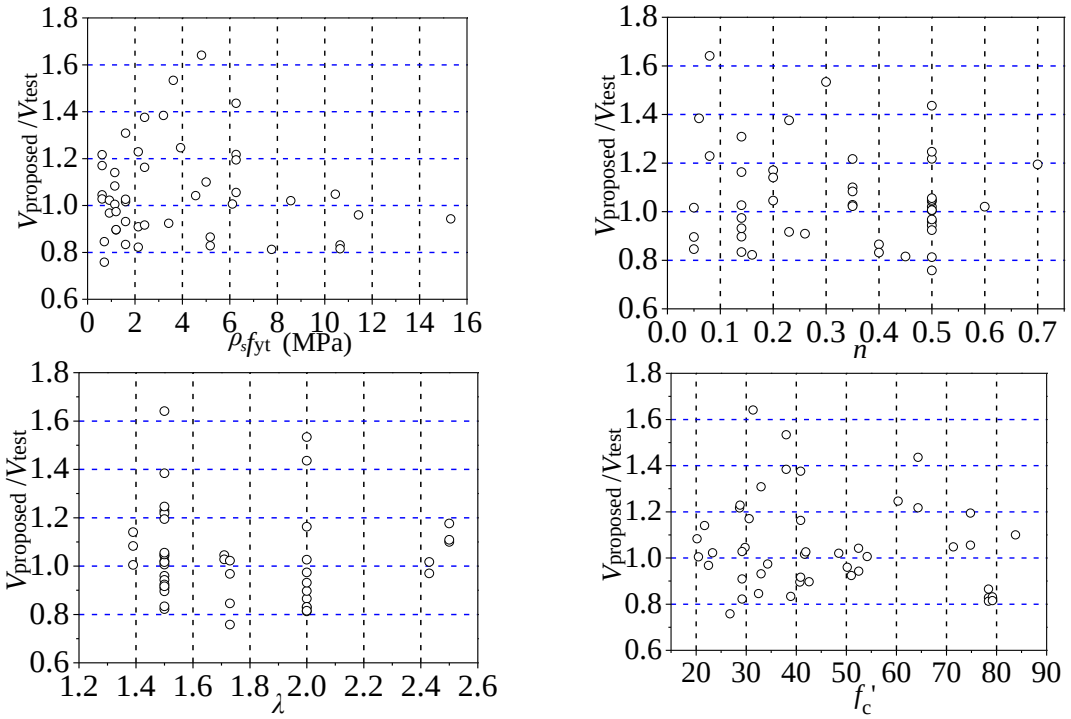

Fig. 11 Variation of the experimental to predicted strength ratio as a function of key parameters

Code and ACI 318-08 models are sensitive to the yielding strength of transverse reinforcement. Because the models ignore a very important fact that the strength of stirrups is not always fully developed in actual concrete members, especially for members confined with high-strength stirrups or high transverse reinforcement ratio. Under conditions of transverse reinforcement ratio larger than 1.2% or transverse reinforcement index $\rho_s f_{yv}$ larger than 4.0, there is no yielding in transverse reinforcement (1990a, 2010d). Therefore, the contribution of transverse reinforcement is overestimated in shear strength computation for the Chinese code and ACI 318-08 models. Among the three shear strength methods mentioned above, the proposed method gives the best match with the experimental results from the database.

To investigate the validity and applicability of the proposed equation, the ratio of shear strength $V_{proposed}/V_{test}$ against transverse reinforcement index, axial load ratio, shear span-depth ratio and concrete compressive strength are shown in Fig. 11. The good correlation between the experimental and the calculated shear strengths across the range of transverse reinforcement index, axial compression ratio, shear span ratio and concrete compressive strength demonstrates that the proposed method can well represent the effects of these key parameters. Therefore, it can be concluded that the proposed shear strength method is applicable and reliable.

5. Conclusions

An experimental program was carried out on six high-strength concrete columns under cyclic double curvature bending and constant axial load. The seismic performance of specimens was

discussed. Shear strength formula of short columns, which experienced a splitting failure, was proposed based on Chinese concrete code. The conclusions can be drawn as follows:

• All specimen columns failed with the development of vertical cracks forming along the longitudinal reinforcing bars located at mid-height of the column sections. This vertical splitting spread through the interior of the specimen along inner transverse reinforcement, and separated it into three parts. It was confirmed that the vertical split penetrated the whole section and extended throughout, except at the both ends where the flexural hinge developed.

• By contrast with specimens with normal-strength lateral bars, there was no steep reducing in the shear bearing capacity of specimens with high-strength stirrup after the maximum lateral force was attained. And the yielding strength of transverse reinforcement affects the behavior of RC columns more significant in ductility than in shear strength.

• It is helpful to increase the deformation and energy dissipation capacity of short concrete columns by using high-strength stirrups. For specimens with high-strength hoops, the ductility coefficient is increased by 39.4%, while the ultimate drift is increased by 50.0%. And energy dissipation of columns with high-strength stirrups is increased by 32.9%-310% than those of specimens with normal-strength stirrups.

• When loaded to the maximum shear force, high-strength lateral reinforcing bars did not experience yielding, while, normal-strength transverse reinforcing bars had reached or been closed to the yielding strength. As expected of no yielding, core concrete could still be confined adequately by high-strength stirrups even after peak shear force was attained.

• The contribution of transverse reinforcement to the shear strength of short columns, which experienced a splitting failure, is overestimated by the Chinese concrete code and ACI 318-08 models. A new shear strength equation for columns with a splitting failure was proposed. Comparisons made between shear strength calculated based on the proposed formula and test results screened from literature available showed a good agreement, and the average shear strength ratio and COV were 1.05 and 0.19, respectively.

Acknowledgments

The authors would like to thank the National Natural Sciences Foundation of China (NO. 51178380 and NO. 51478382) and Specialized Research Fund for the Doctoral Program of Higher Education (NO.20116120110004) for their generous financial support of the project. The experimental work described in this paper was carried out in Structure and Seismic Key Laboratory at Xi'an University of Architecture & Technology. The technical assistance and cooperation of the laboratory staff is greatly appreciated.

References

American Concrete Institute (ACI) (2008b), "Building code requirements for structural concrete and commentary", ACI 318 (318R-08), American Concrete Institute, Farmington Hills, MI.

Aoyama, H. (2001a), *Design of Modern Highrise Reinforced Concrete Structures*, Imperial College Press, London, UK.

Bhayusukma, M.Y. and Tsai, K.C. (2014c), "High-strength RC columns subjected to high-axial and increasing cyclic lateral loads", *Earthq. Struct.*, **7**(5), 779-796.

Cagatay, I.H., Beklen, C. and Mosalam, K.M. (2010a), "Investigation of short column effect of RC building:

failure and prevention", *Comput. Concrete*, **7**(6), 523-532.
Caglar, N. and Mutlu, M. (2009), "Failure analysis of reinforced concrete frames with short column effect", *Comput. Concrete*, **6**(5), 403-419.
Chen, C.Y., Liu, K.C., Liu, Y.W. and Huang, W.J. (2010b), "A case study of reinforced concrete short column under earthquake using experimental and theoretical investigations", *Struct. Eng. Mech.*, **36**(2), 197-206.
Guevara, L.T. and García, L.E. (2005a), "The captive- and short-column effects", *Earthq. Spectra*, **21**(1), 141-160.
Gupta, P.R. and Collins, M.P. (2001b), "Evaluation of shear design procedures for reinforced concrete members under axial compression", *Struct. J.*, **98**(4), 537-547.
Harumi, Y., Yasuo, T., Masayuki, N. and Younggon, R. (1990b), "Study on shear failure mechanisms of reinforced concrete short columns", *Eng. Fract. Mech.*, **35**(1-3), 277-289.
Ichinose, T. (1995), "Splitting bond failure of columns under seismic action", *Struct. J.*, **92**(5), 535-542.
Koçak, A. (2013a), "The effect of short columns on the performance of existing buildings", *Struct. Eng. Mech.*, **46**(4), 505-518.
Lura, P., Plizzari, G.A. and Riva, P. (2002), "3D finite-element modeling of splitting crack propagation", *Magaz. Concrete Res.*, **54**(6), 481-493.
Ministry of Housing and Urban-Rural Development of the People's Republic of China (MOHURD) (2010c), "Code for design of concrete structures", GB 50010-2010, MOHURD.
Mohamed, H.H. and Farid, D. (2008a), "Seismic strengthening of bond-critical regions in rectangular reinforced concrete columns using fiber-reinforced polymer wraps", *Struct. J.*, **105**(1), 68-77.
Moretti, M.L. and Tassios, T.P. (2006), "Behavior and ductility of reinforced concrete short columns using global truss model in concrete beams", *Struct. J.*, **103**(3), 319-327.
Pandey, G.R. and Mutsuyoshi, H. (2005b), "Seismic performance of reinforced concrete piers with bond-controlled reinforcements", *Struct. J.*, **102**(2), 295-304.
Paultre, P., Legeron, F. and Mongeau, D. (2001c), "Influence of concrete strength and transverse reinforcement yield strength on behavior of high-strength concrete columns", *Struct. J.*, **98**(4), 490-501.
Pham, T.P. and Li, B. (2013b), "Seismic behavior of RC columns with light transverse reinforcement under different loading directions", *Struct. J.*, **110**(5), 833-844.
Pham, T.P. and Li, B. (2014a), "Splitting failure of reinforced concrete columns", *J. Struct. Eng.*, **140**(3), 1-11.
Pham, T.P. and Li, B. (2014b), "Seismic behavior of RC columns with plain longitudinal reinforcing bars", *Struct. J.*, **111**(3), 561-572.
Sato, H. and Kaminosono, T. (1992), "Vertical splitting failure of high-strength RC columns after flexural yielding", *Earthquake Engineering, Tenth World Conference*, balkerma, Rotterdam.
Shi, Q.X., Yang, W.X., Wang, Q.W., Tian, Y., Zhang, X.H., Jiang, W.S., Bai, L.G. and Zhao, Q.C. (2012b), "Experimental research on seismic behavior of high-strength concrete short columns with high-strength stirrups", *J. Build. Struct.*, **33**(9), 49-58.
Sun, Z.G., Si, B.J., Guo, X., Yu, D.H. and Li, X.L. (2011), "Experimental research on the shear-bond failure of RC columns under seismic action", *Eng. Mech.*, **28**(3), 109-117, 149.
Tran, C. T. N. and Li, B. (2012a), "Initial stiffness of reinforced concrete columns with moderate aspect ratios", *Adv. Struct. Eng.*, **15**(2), 265-276.
高木仁之，田中礼治，狩野芳一(1990a), "高強度鉄筋を用いた.鉄筋コンクリート部材の設計上の問題点-せん断補強筋として利用場合[J]", コンクリート工学，**28**(5).
日本建筑学会(2010d), "鉄筋コンクリート構造計算規準［S］", 同解説.